2020 8th IEEE International Conference on Biomedical
Robotics and Biomechatronics (BioRob)
New York, USA. Nov 29 - Dec 1, 2020

Evidence for Dynamic Primitives in a Constrained Motion Task

James Hermus[1], Dagmar Sternad[2], and Neville Hogan[1,3]

***Abstract*—Ten right-handed male subjects turned a crank (radius 10.29 cm) in two directions at three constant instructed speeds (fast, medium, very slow) with visual speed feedback. They completed 23 trials at each speed. With the hand constrained to move in a circle, non-zero forces against the constraint were measured. Assuming a plausible mathematical model of interactive dynamics, the peripheral neuromechanics could be 'subtracted', revealing an underlying motion that reflected neural control. We called this data-driven construct the zero-force trajectory. The observed zero-force trajectory was approximately elliptical. Its major axis, estimated by the principal eigenvector of the covariance matrix, differed significantly for the two movement directions. As peripheral neuromuscular compliance (i.e. low mechanical impedance) mitigates the consequences of imperfect execution, the required precision of motion commands is reduced. An oscillatory zero-force trajectory that leads hand motion suffices to produce circular hand motions. Due to non-isotropic peripheral dynamics, that lead differs between degrees of freedom, resulting in an elliptical zero-force trajectory. The ellipses' orientations differ with direction of rotation, as observed in the experimental data. As elliptical motion is generated by two non-colinear sinusoids with non-zero phase difference, these results support the hypothesis that humans simplify this constrained-motion task by exploiting primitive dynamic actions, oscillations and impedance.**

I. Introduction

Using tools is a hallmark of human behavior, comparable to language and laughter. While some animals are capable of making and using tools, this ability is vastly more developed in humans [1]–[4]. Nonetheless, neuroscience research has primarily focused on the examination of elementary behaviors under strict experimental control (unconstrained motion). While these paradigms render manageable data for analysis and modeling, it is difficult to generalize the insights to understand the actions that make humans special—tool use. Physical interaction with a kinematic constraint provides an intermediate stage between unconstrained motion and physical interaction with complex dynamic objects. Moreover, kinematic constraints are ubiquitous in everyday object manipulation. Activities such as turning a steering wheel, or opening a door, are aspects of everyday life which humans perform effortlessly. This paper presents a study of unimpaired subjects physically interacting with a circular constraint—turning a crank.

While human dexterity vastly exceeds that of most modern robots, the human neuro-mechanical system is remarkably slower than its robotic counterparts [5]. We have proposed that, to achieve highly dynamic performance despite these limitations, human behavior is composed of *dynamic primitives* [6]–[12]. We conceive these to be dynamic attractors that emerge from nonlinear interactions between neural and mechanical parts of the system and require minimal intervention from higher levels of the central nervous system. In this work, we discuss two types of dynamic primitives: oscillations and mechanical impedance.

In a task that involves significant physical interaction, the mechanical impedance (interactive dynamics) of the limb relates the descending neural commands, the motion of the hand, and the force on the hand. Thus, looking at any one of these quantities without considering the influence of the others would only partially explain the action.

In a previous work, we presented a novel method [13]. The approach assumed a plausible mathematical model of interactive dynamics and used it to 'subtract off' or 'peel back' peripheral biomechanics to uncover a summary of the underlying neural influences. We defined this quantity as the *zero-force trajectory*, one consequence of the underlying neural commands. The previous work also showed that patterns believed to be the result of neural control re-emerge in the zero-force trajectory.

Slow neural transmission and muscle response implies that humans rely heavily on feed-forward (i.e. predictive) control; prior work shows that humans adjust their behavior to prioritize predictability [14]–[18]. In theory, strictly periodic actions are infinitely predictable. Negotiating a circular constraint at constant tangential speed (equivalently: constant angular speed) requires periodic hand motion in each degree of freedom. For these reasons, we anticipate that crank-turning might preferentially be executed as an oscillatory action. Here we studied circularly constrained hand motion at constant tangential speed.

This work re-examined the zero-force trajectory estimates reported previously [13]. However, a different hypothesis was tested. This work theorized that humans use dynamic primitives, oscillations and impedance, to accomplish this constrained-motion task. This led to a testable prediction: The zero-force trajectory will exhibit differences between directions of motion. Constant-speed circular hand motion requires sinusoidal motion in orthogonal directions with a phase offset of ±90° (the sign depends on the direction CW vs. CCW). However, the motion of the hand would lag the neurally-defined zero-force trajectory to an extent determined by the slow response of the bio-mechanical periphery. This lag is likely to differ in orthogonal directions, resulting in different performance between the CW and CCW directions. The zero-force trajectory is one consequence of the underlying neural commands. Thus, if the zero-force trajectory is composed of oscillations, it should exhibit differences as a function of turning direction.

Results showed that the zero-force trajectory was approximately elliptical at the medium and fast speeds, while nearly circular at the very slow speed. The principal eigenvector of its best-fit covariance matrix served as a measure of major axis orientation of the ellipse. As predicted, turning direction had a significant effect on the ellipse orientation. This observation is consistent with the hypothesis that (at the medium and fast speed) this constrained motion

978-1-7281-5907-2/20/$31.00 ©2020 IEEE

task was performed by a combination of two dynamic primitives -- oscillations and mechanical impedance.

II. Methods

A. Participants

Ten healthy male college-age students were recruited for the study. All participants were right-handed, and none reported any biomechanical injury to their arm nor any neurological problems. Prior to participating in the study, they were informed about the experimental procedure and signed the informed consent document approved by MIT's Institutional Review Board.

B. Experimental Apparatus and Procedure

The crank used in this experiment is shown in Figure 1. The crank arm was mounted on a high precision incremental optical encoder/interpolator set (Gurley Precision Instruments encoder #8335-11250-CBQA, interpolator #HR2-80 QA-BRD) with a resolution of 0.0004 degrees per count. A six-axis force transducer (ATI Model 15/50) was attached to the end of the crank, with a handle mounted on it. A spool managed the force transducer cable.

During the experiment, the subject's arm was occluded from view by a wooden panel, which did not affect the range of motion. The arm and forearm were suspended in the plane of the crank by a canvas sling. The subject sat in a chair with a rigid back. The wrist was braced and the shoulder was constrained by a harness attached to the back of the chair. The subject was positioned such that the crank, with radius 10.29 cm, was well within the workspace of the arm.

Data acquisition was controlled by a computer running the QNX real-time operating system on an Intel Pentium 100 processor. The encoder, sampling at 200 Hz, was connected to a set of counters and to the computer via digital I/O. The ATI force transducer's signal, sampled at 100 Hz, was processed by its embedded controller and input to the computer through the digital I/O. The visual display, also generated by the computer, was on a 17-inch monitor (311 x 238 mm, resolution 1280 x 1024, 76 Hz) which was mounted approximately 75 cm from subjects' eyes. The experiment was divided into two unequal sections: 2 blocks of trials at subjects' preferred or 'comfortable' speed and 6 blocks of trials at a visually-instructed speed.

At the start of the experiment, subjects performed 20 trials at their preferred speed, 10 trials in the CW direction and 10 in the CCW direction; both conditions were blocked, in random sequence for each subject; each trial lasted 8 seconds. Subjects were not provided any visual feedback during these trials. Thereafter, subjects performed 6 blocks of 30 trials, each with visual specification of 1 of 3 target speeds (slow: 0.075, medium: 0.5, and fast: 2.0 revolutions per second), in either CW or CCW directions. The order of the speed and direction blocks was pseudo-randomized across subjects. The three speeds were selected to cover a significant range: 0.075 rev/s was extremely slow (required over 13 s per revolution), 0.5 rev/s was close to subjects' preferred speed, and 2.0 rev/s was close to the fastest speed that subjects could turn the crank. Visual feedback on the monitor displayed the target speed, as well as subjects' real-time hand speed; the horizontal axis was time, and the vertical axis was speed. Subjects' speed was estimated using an online backward finite difference algorithm. Target speed was displayed as a continuous horizontal line in the middle of the screen. The relation between crank speed and screen display was re-scaled for every block; the width of the screen corresponded to the time of the trial, which was a function of the desired crank speed.

In the slow-speed conditions, each trial lasted 45 s; in the medium-speed conditions, each trial lasted 16 s; in the fast-speed conditions, each trial lasted 4 s. This yielded 8 turns of the crank for the fast and medium conditions, but only about 3.4 turns of the crank for the slow condition. The duration of the slow-speed trials was limited to avoid subject fatigue.

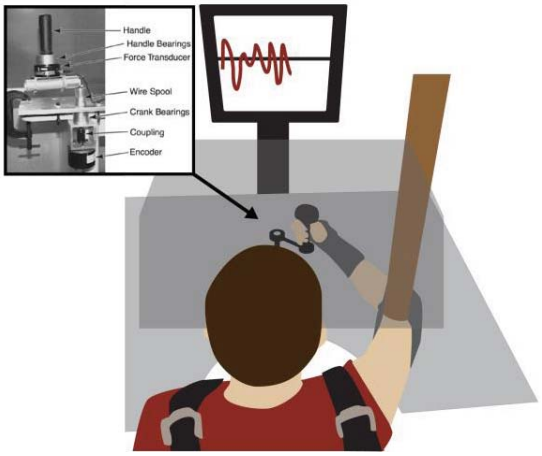

Figure 1: Experimental setup. The crank displayed in the inset was used to provide a circular constraint. Vision of the arm and crank was occluded but the subject was provided with visual speed feedback. The wrist was braced, the elbow was supported by a sling, and the shoulders were strapped to a chair.

C. Model

The arm was modeled as a two-link planar manipulator, with no gravitational effects. Inertia parameters were estimated based on the results of the cadaver studies of Dempster [19], [20]. The shoulder joint location was modeled as a fixed point, as the thorax and scapula were assumed to be stationary. The two-link manipulator dynamics coupled to the crank is detailed in the Appendix. This approach is the same as used by Ohta et al. [21].

Though muscle force production is a complex function of many factors, its dominant behavior can be well described by a function of muscle length and its rate of change [22], [23]. One way to describe the dynamics of interaction uses a mechanical impedance operator $Z\{\cdot\}$ [24]. The force $F(t)$ time-function can be computed from the displacement time-function $\Delta x(t)$, $F(t) = Z\{\Delta x(t)\}$. Displacement is defined as $\Delta x(t) = x_0(t) - x(t)$ where $x(t)$ is the actual hand position and $x_0(t)$ is a zero-force trajectory. Accordingly, a simplified model of muscle mechanical impedance was used—a linear spring and viscous damping element with common motion [25]. To implement this model on a two-joint arm, joint stiffness was assumed to be a 2×2 symmetric matrix, independent of configuration. Joint damping, also a 2×2 symmetric matrix, was proportional to joint stiffness. This is similar to the muscle model previously used by Flash [26] but

in this case we used a damping term which was defined relative to the zero-force trajectory.

The joint torque was defined by,

$$\boldsymbol{\tau} = \boldsymbol{K}(\boldsymbol{q}_0 - \boldsymbol{q}) + \boldsymbol{B}(\dot{\boldsymbol{q}}_0 - \dot{\boldsymbol{q}}) \quad (1)$$

The stiffness in units of N-m/rad was defined as

$$\boldsymbol{K} = G\begin{bmatrix} K_{11} & K_{12} \\ K_{21} & K_{22} \end{bmatrix} = G\begin{bmatrix} 29.5 & 14.3 \\ 14.3 & 39.3 \end{bmatrix} \quad (2)$$

The viscous damping in units of N-m-s/rad was defined as

$$\boldsymbol{B} = \begin{bmatrix} B_{11} & B_{12} \\ B_{21} & B_{22} \end{bmatrix}. \quad (3)$$

The K_{11} and B_{11} terms are the net shoulder joint stiffness and damping, the K_{12}, B_{12}, K_{21}, and B_{21} are the two-joint parameters, and the K_{22} and B_{22} terms describe the elbow parameters. The term G is a dimensionless scalar. The values for joint stiffness and damping were consistent with those of Flash [26], such that $\boldsymbol{B} = \beta\boldsymbol{K}$. The β term has units of time, consistent with a first-order model of muscle impedance. A gain of $G = 0.5$ was used in the slow and medium cases, and a gain of $G = 1.5$ was used in the fast case. Damping was derived from stiffness by multiplication by a constant factor, β, which was 0.05 s for the slow and medium cases, and 0.1 s for the fast cases.

Substituting Equation 1, into Equation 9, 10, and 11 (see Appendix), the equation can be manipulated to solve for $\dot{\boldsymbol{q}}_0$.

$$\begin{aligned}\dot{\boldsymbol{q}}_0 = \boldsymbol{B}^{-1}[\boldsymbol{M}\boldsymbol{J}^{-1}[\{\boldsymbol{J}\boldsymbol{M}^{-1}\boldsymbol{J}^T + r^2 I^{-1}\boldsymbol{e}\boldsymbol{e}^T\}\boldsymbol{F} - \dot{\boldsymbol{J}}\dot{\boldsymbol{q}} \\ -r\dot{\theta}\left(\dot{\theta}\boldsymbol{n} + b_c I^{-1}\boldsymbol{e}\right)] + \boldsymbol{h} - \boldsymbol{K}(\boldsymbol{q}_0 - \boldsymbol{q})] + \dot{\boldsymbol{q}}\end{aligned} \quad (4)$$

Numerically integrating this first-order differential equation, (Equation 4) computes the zero-force trajectory corresponding to a prescribed position, velocity, acceleration, and force.

The velocity and force signals were filtered with a second-order Butterworth filter using a cutoff frequency of 10 Hz, except in the slow tangential force condition. The tangential force at the slow speed was small in magnitude because there was a large number of samples with a magnitude close to the resolution of the sensor. This resulted in artifactual step changes in the force measurements. To eliminate this artifact, the tangential force in the slow condition was filtered with a cutoff frequency of 0.5 Hz, far faster than the turning frequency of the slow task (0.075 rev/sec).

D. Covariance Ellipse Orientation

To test whether the zero-force trajectory consistently changed orientation as a function of speed and direction, the zero-force trajectory covariance was computed,

$$cov(x_0, y_0) = \frac{1}{N}\sum_{i=1}^{N}(x_{0,i} - \mu_{x,0})(y_{0,i} - \mu_{y,0}) \quad (5)$$

where x_0 and y_0 are the Cartesian zero-force trajectory points, μ_{x_0} and μ_{y_0} are the mean Cartesian zero-force trajectory points, and N is the number of samples. The eigenvectors of this covariance matrix were computed to determine the major and minor axes of the covariance ellipse. The ellipse orientation was measured relative to the 6 o'clock position, and the sign of the measurement depended on turning direction (illustrated in the inset of Figure 3). The first trial for each condition was excluded. In all subsequent trials, the first 1.5 s were discarded to remove any transient effects induced by the initial condition specified for numerical integration. Only complete revolutions were included. The dependent measure submitted to statistical analysis was the angle of the covariance ellipse of the zero-force trajectory. When the ratio between the major and minor axis of the ellipse approaches unity, the orientation of the major axis angle is ill-defined. This was the case for many of the slow speed trials. As a result, the statistical analysis was only performed on the medium and fast speed trials. To statistically evaluate the influence of speed and direction, a linear mixed model was employed; it was then tested using analysis of variance (ANOVA). The linear model which represents the observed dependent measure $Y_{i,j,k}$ was expressed as

$$\begin{aligned}Y_{i,j,k} = \mu_T + \alpha_j + \beta_k + \gamma_l + (\alpha\beta)_{j,k} + (\alpha\gamma)_{j,l} \\ +(\beta\gamma)_{k,l} + (\alpha\beta\gamma)_{j,k,l} + E_{i,(j,k,l)}\end{aligned} \quad (6)$$

where the grand mean is μ_T, the fixed effect of speed is α_j, where j is an index from 1 to 2. The fixed effect of direction is β_k, where k is an index from 1 to 2. The random effect of subject is γ_l, where l is an index from 1 to 10. The stochastic sampling effect is $E_{i,j,k}$, where i is an index from 1 to 22, representing the multiple trials.

III. Results

In this experiment subjects turned the planar crank at different speeds either in the CW or in the CCW direction. Our working hypothesis was that this task was executed via dynamic primitives. Extracting the zero-force trajectory as one consequence of the underlying neural commands, we could test the following prediction: the zero-force trajectory would be oscillatory, and exhibit differences between directions due to the phase lag introduced by peripheral neuro-mechanical dynamics.

A. Covariance Ellipse Orientation

Figure 2 displays a representative zero-force trajectory from one subject in each direction and speed condition. The shapes are approximately elliptical and show consistent speed fluctuations along the ellipse. Previous work also reported that speed minima coincide with curvature maxima [13]. In addition, this analysis shows that the elliptic shapes clearly displayed a difference in orientation between the two directions. To quantitatively test whether the orientation differed with respect to speed or direction, the major axis angle of the covariance ellipse was computed (Figure 3). The mean major axis angle in the CW conditions were 129.33 ± 16.16^o (medium) and 116.37 ± 2.67^o (fast). The mean major axis angle in the CCW conditions were 168.11 ± 17.86^o (medium) and 158.31 ± 4.31^o (fast). A significant main effect of speed ($F_{1.0,9.0} = 13.135$, $p = 0.001$) and direction ($F_{1.0,9.0} = 64.668$, $p << 0.001$) was detected.

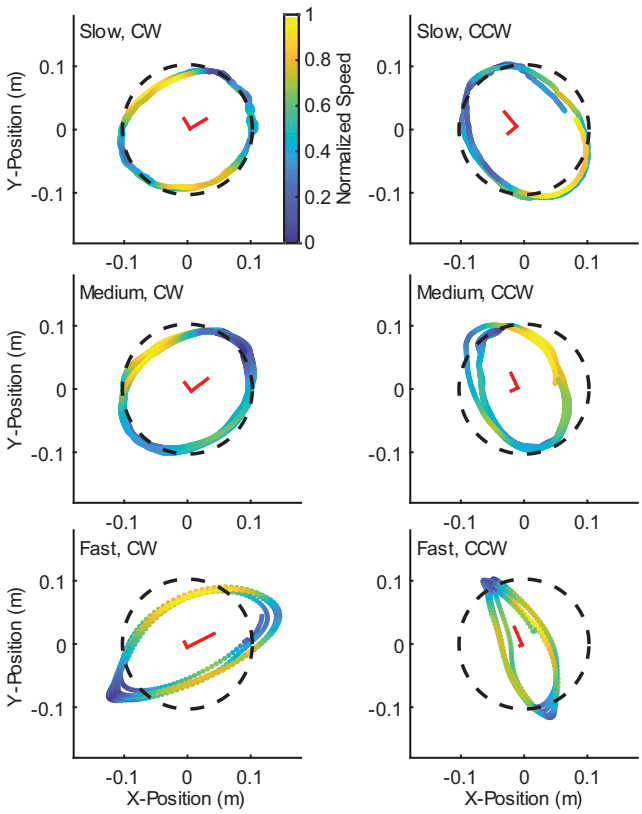

Figure 2: One representative trial from one subject in each of the slow, medium, and fast speed conditions. Top: slow speed; middle: medium speed; bottom: fast speed. Left: clockwise direction trials; Right: counter-clockwise direction trials. The path defined by the constraint is shown by the black dashed circle. The zero-force trajectories are shown by lines with varying color that indicates speed along the zero-force path (normalized by its range). Importantly, the zero-force trajectory is roughly elliptical and that orientation differs with direction.

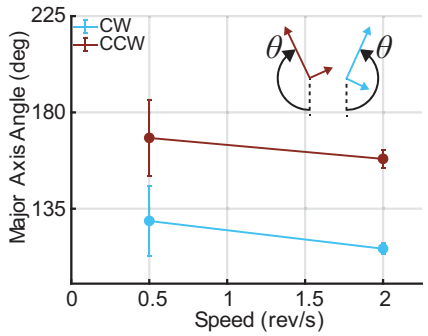

Figure 3: To quantify the orientation of the elliptical zero-force trajectory the covariance ellipse was computed. The plot displays the mean angle of the major axis of the covariance ellipse as a function of turning speed and direction. Error bars indicate the standard deviation between subjects.

IV. Discussion

This study examined kinematically constrained motion as an intermediate step to bridge the gap between (widely-studied) unconstrained motions and (sparsely-studied) physical interaction with objects with complex dynamics. We investigated the detailed patterns of motion and force that human subjects exhibited when performing a simple constrained-motion task, turning a circular crank. Performing this task using oscillatory dynamic primitives would require two sinusoids with non-zero phase difference, specifically ±90° out of phase for moving in a circle. Rather than attempt to execute a perfect circle, low mechanical impedance, another dynamic primitive, would obviate the need for precise motion control. However, the resulting peripheral neuro-mechanical dynamics would contribute a different phase lag in orthogonal directions. We therefore expected differences when subjects turned in opposite directions, and that was observed.

We assumed a simplified model of neuro-muscular mechanical impedance and used it to 'peel back' peripheral neuro-mechanics, and 'reveal' a consequence of underlying neural commands, expressed in terms of motion—the zero-force trajectory. The zero-force trajectory is mathematically similar to the 'virtual trajectory' of the equilibrium point hypothesis [27]–[29]. However, unlike the virtual trajectory, we are agnostic about whether the CNS encodes this quantity; many alternatives might yield similar results. Instead, the zero-force trajectory is a construct based on the measured force and motion, in combination with a reasonable, albeit simplified, model of peripheral neuro-mechanics.

The zero-force trajectory was roughly elliptical. We determined the orientation of its major axis via the principal eigenvector of the covariance matrix. Remarkably, we found that direction (CW vs. CCW) had a substantial and significant effect. This direction dependence was consistent with a neurally-defined motion command (the zero-force trajectory) composed of two sinusoids with a non-zero phase difference.

A model that accounts for the anisotropy of skeletal inertia and neuro-muscular impedance was sufficient to explain these results. Consider the simple system where the zero-force trajectory in two orthogonal directions, x_0 and y_0, is constructed from two out of phase sinusoids with the same frequency, Ω, same magnitude, and a phase difference, ϕ.

$$\begin{cases} x_0 = \sin(\Omega t) \\ y_0 = \sin(\Omega t + \phi) \end{cases} \tag{7}$$

Given such a system, a perfect circle can be drawn in the CW or CCW direction with a phase difference of ±90°. However, we know that peripheral neuro-mechanical dynamics contribute a different phase lag in different directions. The apparent mass of a two-link manipulator in the work-space is not uniform; the eigenvalues of the mass matrix are not equal. This direction-dependent variation of apparent mass is one cause of the different phase lags in different directions of motion. The additional phase lag contributed by peripheral neuro-mechanical dynamics results in zero-force trajectories with an elliptical shape that is oriented differently for CW and CCW motion. In fact, this directional effect is consistent with the change in orientation of the zero-force trajectory that we observed in our experiments.

V. Conclusion

Despite its apparent simplicity, this constrained-motion task evoked a rich set of behaviors. We observed directional differences in the zero-force trajectory orientation, consistent with task execution generated by dynamic primitives. Our observations indicate that subjects took advantage of

interactive dynamics (hand mechanical impedance) to manage the control of contact and avoid the need for precise force control. The underlying motion that generated force via mechanical impedance was competently described by two oscillatory dynamic primitives, phase-shifted sinusoids. These results provide further evidence that humans manage complex physical interaction tasks by taking advantage of dynamic primitives, in this case oscillations and impedance.

VI. Appendix

The model of the arm and crank system was constructed in the same manner as performed by Ohta et al. [21]. Figure 4 displays the variables and notation used in the development of the model. Inertia parameters were estimated based on the results of the cadaver studies of Dempster [19], [20].

The system has one degree of freedom; therefore, there is always a kinematic relation that can be used to transform from Cartesian position, $\boldsymbol{x} = [x, y]^T$, to joint position, $\boldsymbol{q} = [q_1, q_2]^T$, and to crank position, θ, where the center of the crank is defined as $\boldsymbol{x_c} = [x_c, y_c]$.

$$\boldsymbol{x} = \begin{bmatrix} \mathrm{l}_1\mathrm{C}_1 + \mathrm{l}_2\mathrm{C}_{12} \\ \mathrm{l}_1\mathrm{S}_1 + \mathrm{l}_2\mathrm{S}_{12} \end{bmatrix} = \begin{bmatrix} \mathrm{r}\cos\theta \\ \mathrm{r}\sin\theta \end{bmatrix} + \boldsymbol{x}_c \qquad (8)$$

The notation S_1, C_1 denote $\sin(q_1)$, $\cos(q_1)$ and S_{12}, C_{12} denote $\sin(q_1 + q_2)$, $\cos(q_1 + q_2)$. The radius of the crank is r, the damping of the crank is b_c, and the inertia is I. The upper arm, denoted by 1, and the forearm plus hand, denoted by 2, are described by length l_1, l_2, mass m_1, m_2, inertia about the z axis I_1, I_2, and center of mass distance from the joint axis c_1, c_2. Limb parameters are reported in previous work [13]. The inertia of the crank about the pivot was 3.716×10^{-3} kg/m. The force on the handle is $\boldsymbol{F} = [F_x, F_y]^T$, with the normal unit vector, $\boldsymbol{n}$ and tangential unit vector, $\boldsymbol{e}$. The joint torque is denoted $\boldsymbol{\tau} = [\tau_1, \tau_2]^T$.

From the sum of moments acting on the crank,

$$I\ddot{\theta} + b_c\dot{\theta} = r\boldsymbol{e}^T\boldsymbol{F} \qquad (9)$$

summation of moments about the shoulder,

$$\boldsymbol{M}\ddot{\boldsymbol{q}} + \boldsymbol{h} = \boldsymbol{\tau} - \boldsymbol{J}^T\boldsymbol{F} \qquad (10)$$

and the kinematic relation that equates the acceleration at the handle to the acceleration at the hand,

$$\ddot{\boldsymbol{x}} = \boldsymbol{J}\ddot{\boldsymbol{q}} + \dot{\boldsymbol{J}}\dot{\boldsymbol{q}} = r(\ddot{\theta}\boldsymbol{e} - \dot{\theta}^2\boldsymbol{n}) \qquad (11)$$

and the joint torque defined by in Equation 1, a model of the system can be constructed. Substituting Equation 1, into Equation 9, 10, and 11, the equations can be manipulated to solve for $\dot{\boldsymbol{q}}_0$ (see Equation 4). Parameters comprising these equations include the mass matrix, the centrifugal and Coriolis forces, and the Jacobian relating unconstrained differential arm motions to hand motions.

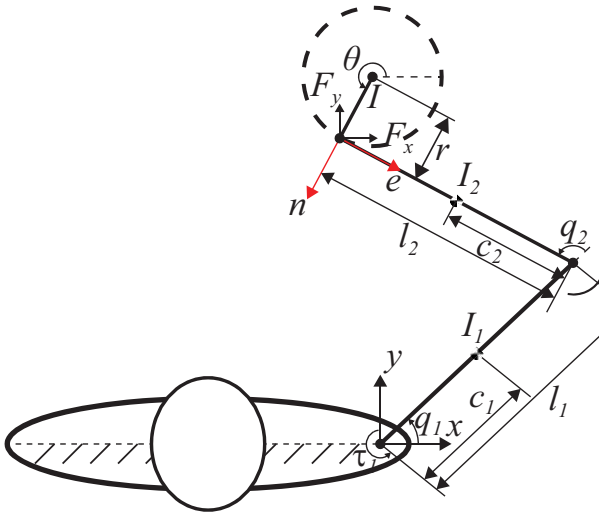

Figure 4: Model of crank rotation task which displays the sign convention and notation used in the computations.

Acknowledgment

We would like to thank Joseph Doeringer for data collection.

References

[1] G. R. Hunt, "Manufacture and use of hook-tools by new caledonian crows," *Nature*, vol. 379, no. 6562, pp. 249–251, Jan. 1996.

[2] B. Kenward, A. A. S. Weir, C. Rutz, and A. Kacelnik, "Behavioural ecology: tool manufacture by naive juvenile crows," *Nature*, vol. 433, no. 7022, pp. 121–121, Jan. 2005.

[3] C. Boesch and H. Boesch, "Tool use and tool making in wild chimpanzees.," *Folia Primatol.*, vol. 54, no. 1–2, pp. 86–99, 1990.

[4] S. H. Johnson-Frey, "The neural bases of complex tool use in humans," *Trends Cogn. Sci.*, vol. 8, no. 2, pp. 71–78, Feb. 2004.

[5] E. Kandel, J. Schwartz, T. Jessell, S. Siegelbaum, and A. J. Hudspeth, *Principles of neural science*, 5th Ed. McGraw-Hill, 2013.

[6] S.-W. Park, H. Marino, S. K. Charles, D. Sternad, and N. Hogan, "Moving slowly is hard for humans: limitations of dynamic primitives," *J. Neurophysiol.*, vol. 118, no. 1, pp. 69–83, 2017.

[7] N. Hogan, "Physical interaction via dynamic primitives," in *Geometric and numerical foundations of movements*, J.-P. Laumond, N. Mansard, and J.-B. Lasserre, Eds. Springer, 2017, pp. 269–299.

[8] N. Hogan and D. Sternad, "On rhythmic and discrete movements: reflections, definitions and implications for motor control," *Exp. Brain Res.*, vol. 181, no. 1, pp. 13–30, 2007.

[9] N. Hogan and D. Sternad, "Dynamic primitives of motor behavior," *Biol. Cybern.*, vol. 106, no. 11–12, pp. 727–739, Dec. 2012.

[10] D. Sternad, "Towards a unified theory of rhythmic and discrete movements — behavioral, modeling and

imaging results," in *Coordination: Neural, Behavioral and Social Dynamics*, Berlin, Heidelberg: Springer Berlin Heidelberg, 2008, pp. 105–133.
[11] S. Schaal, S. Kotosaka, and D. S. Robotics, "Nonlinear dynamical systems as movement primitives," in *Conference on humanoid robotics*, 2000, pp. 1–11.
[12] D. Sternad, W. J. Dean, and S. Schaal, "Interaction of rhythmic and discrete pattern generators in single-joint movements," *Hum. Mov. Sci.*, vol. 19, no. 4, pp. 627–664, Oct. 2000.
[13] J. R. Hermus, J. Doeringer, D. Sternad, and N. Hogan, "Separating neural influences from peripheral mechanics: the speed-curvature relation in mechanically-constrained actions," *J. Neurophysiol.*, vol. 123, pp. 1870–1885, 2020.
[14] P. Maurice, N. Hogan, and D. Sternad, "Predictability, force, and (anti)resonance in complex object control," *J. Neurophysiol.*, vol. 120, no. 2, pp. 765–780, Aug. 2018.
[15] D. Sternad, "Human control of interactions with objects – variability, stability and predictability," in *Geometric and numerical foundations of movements*, J.-P. Laumond, N. Mansard, and J.-B. Lasserre, Eds. Springer, 2017, pp. 301–335.
[16] B. Nasseroleslami, C. J. Hasson, and D. Sternad, "Rhythmic manipulation of objects with complex dynamics: predictability over chaos," *PLOS Comput. Biol.*, vol. 10, no. 10, pp. 1–19, Mar. 2014.
[17] S. Bazzi, J. Ebert, N. Hogan, and D. Sternad, "Stability and predictability in human control of complex objects," *Chaos An Interdiscip. J. Nonlinear Sci.*, vol. 28, no. 10, p. 103103, Oct. 2018.
[18] S. Bazzi and D. Sternad, "Human manipulation of dynamically complex objects through control contraction metrics," *IEEE Robot. Autom. Lett.*, vol. 5, pp. 2578–2585, 2020.
[19] D. I. Miller and R. C. Nelson, *Biomechanics of Sport: a research aproach*. Philadelphia: Lee and Febiger, 1973.
[20] S. Plagenhoef, *Patterns of Human Motion: A Cinematographic Analysis*. Englewood Cliffs, NY: Prentice-Hall, 1971.
[21] K. Ohta, M. M. Svinin, Z. Luo, S. Hosoe, and R. Laboissière, "Optimal trajectory formation of constrained human arm reaching movements," *Biol. Cybern.*, vol. 91, no. 1, pp. 23–36, 2004.
[22] G. C. Joyce, P. M. H. Rack, and D. R. Westbury, "The mechanical properties of cat soleus muscle during controlled lengthening and shortening movements," *J. Physiol.*, vol. 204, no. 2, pp. 461–474, Oct. 1969.
[23] P. M. H. Rack and D. R. Westbury, "The effects of length and stimulus rate on tension in the isometric cat soleus muscle," *J. Physiol.*, vol. 204, no. 2, pp. 443–460, Oct. 1969.
[24] N. Hogan, "Impedance control: an approach to manipulation: part II—implementation," *J. Dyn. Syst. Meas. Control*, vol. 107, no. 1, pp. 8–16, Mar. 1985.
[25] N. Hogan, "An organizing principle for a class of voluntary movements," *J. Neurosci.*, vol. 4, no. 11, pp. 2745–2754, 1984.
[26] T. Flash, "The control of hand equilibrium trajectories in multi-joint arm movements," *Biol. Cybern.*, vol. 57, no. 4, pp. 257–274, 1987.
[27] E. Bizzi, N. Accornero, W. Chapple, and N. Hogan, "Arm trajectory formation in monkeys," *Exp. Brain Res.*, vol. 46, no. 1, pp. 139–143, Apr. 1982.
[28] A. G. Feldman, "Once more on the equilibrium-point hypothesis (lambda model) for motor control.," *J. Mot. Behav.*, vol. 18, no. 1, pp. 17–54, Mar. 1986.
[29] A. G. Feldman, "Functional tuning of the nervous system during control of movement or maintenance of a steady posture. II. Controllable paramaters of the muscles.," *Biophysics*, vol. 11, pp. 565–578, 1966.